Available online at www.sciencedirect.com

SCIENCE DIRECT

Remote Sensing of Environment 91 (2004) 256–270

Remote Sensing of Environment

www.elsevier.com/locate/rse

Modeling gross primary production of temperate deciduous broadleaf forest using satellite images and climate data

Xiangming Xiao[a,*], Qingyuan Zhang[a], Bobby Braswell[a], Shawn Urbanski[b], Stephen Boles[a], Steven Wofsy[b], Berrien Moore III[a], Dennis Ojima[c]

[a] *Complex System Research Center, Institute for the Study of Earth, Oceans and Space, University of New Hampshire, Durham, NH 03824, USA*
[b] *Department of Earth and Planetary Sciences, Harvard University, Cambridge, MA 02138, USA*
[c] *Natural Resources Ecology Laboratory, Colorado State University, Fort Collins, CO 80523, USA*

Received 31 December 2003; received in revised form 23 March 2004; accepted 27 March 2004

Abstract

Net ecosystem exchange (NEE) of CO_2 between the atmosphere and forest ecosystems is determined by gross primary production (GPP) of vegetation and ecosystem respiration. CO_2 flux measurements at individual CO_2 eddy flux sites provide valuable information on the seasonal dynamics of GPP. In this paper, we developed and validated the satellite-based Vegetation Photosynthesis Model (VPM), using site-specific CO_2 flux and climate data from a temperate deciduous broadleaf forest at Harvard Forest, Massachusetts, USA. The VPM model is built upon the conceptual partitioning of photosynthetically active vegetation and non-photosynthetic vegetation (NPV) within the leaf and canopy. It estimates GPP, using satellite-derived Enhanced Vegetation Index (EVI), Land Surface Water Index (LSWI), air temperature and photosynthetically active radiation (PAR). Multi-year (1998–2001) data analyses have shown that EVI had a stronger linear relationship with GPP than did the Normalized Difference Vegetation Index (NDVI). Two simulations of the VPM model were conducted, using vegetation indices from the VEGETATION (VGT) sensor onboard the SPOT-4 satellite and the Moderate Resolution Imaging Spectroradiometer (MODIS) sensor onboard the Terra satellite. The predicted GPP values agreed reasonably well with observed GPP of the deciduous broadleaf forest at Harvard Forest, Massachusetts. This study highlighted the biophysical performance of improved vegetation indices in relation to GPP and demonstrated the potential of the VPM model for scaling-up of GPP of deciduous broadleaf forests.

Keywords: Remote sensing; MODIS; VEGETATION; CO_2 flux tower

1. Introduction

The seasonal variations of gross primary production (GPP) and ecosystem respiration (R) determine net ecosystem exchange (NEE) of CO_2 between the atmosphere and forest ecosystems. In the past decades, researchers in ecosystem science have focused on net primary production (NPP) of ecosystems, which is the difference between GPP and autotrophic respiration (R_a). In recent years, continuous CO_2 flux measurements between forests and the atmosphere at flux tower sites (Wofsy et al., 1993) have allowed for a more detailed examination of the photosynthetically active period (leaf phenology) and GPP of forest ecosystems (Falge et al., 2002a, 2002b). It is thought that even modest changes in the length or magnitude of the plant growing season could result in large changes in annual GPP in deciduous broadleaf forests (Goulden et al., 1996). An analysis of NEE from 1991–2000 in Harvard Forest also suggested that weather and seasonal climate (e.g., light, temperature and moisture) regulated seasonal and interannual fluctuations of carbon uptake in a temperate deciduous broadleaf forest (Barford et al., 2001). Forest CO_2 flux tower sites provide integrated CO_2 flux measurements over footprints with sizes and shapes (linear dimensions typically ranging from hundreds of meters to 1 km) that vary with the tower height, canopy physical characteristics and wind velocity. Regional extrapolation of those CO_2 flux measurements is a challenging task because of the large spatial heterogeneity and temporal dynamics of forest ecosystems across complex landscapes and regions.

* Corresponding author. Tel.: +1-603-862-3818; fax: +1-603-862-0188.
E-mail address: xiangming.xiao@unh.edu (X. Xiao).

0034-4257/$ - see front matter © 2004 Elsevier Inc. All rights reserved.
doi:10.1016/j.rse.2004.03.010

One approach to scale-up and extrapolate site-specific measurements (e.g., GPP, NPP, NEE) is to use process-based biogeochemical models, driven by a multi-layer database of climate, soil and vegetation types (Churkina et al., 2003; Law et al., 2000). CO_2 flux data from the tower sites are useful for parameterization and validation of biogeochemical models. The other scaling-up approach for regional analysis is to use satellite observations and climate data (Turner et al., 2003a; Xiao et al., 2004). A number of satellite-based modeling studies (Behrenfeld et al., 2001; Field et al., 1995; Potter et al., 1993; Prince & Goward, 1995; Ruimy et al., 1994, 1996; Turner et al., 2003a) have used the Production Efficiency Model (PEM) to estimate GPP or NPP at large spatial scales:

$$\mathrm{GPP} = e_g \times \mathrm{FAPAR} \times \mathrm{PAR} \quad (1)$$

$$\mathrm{NPP} = e_n \times \mathrm{FAPAR} \times \mathrm{PAR} \quad (2)$$

where PAR is the incident photosynthetically active radiation (PAR, MJ/m^2) in a time period (e.g., day, month), FAPAR is the fraction of absorbed PAR by the vegetation canopy, e_g is the light use efficiency (LUE, g C MJ^{-1} PAR) in the GPP calculation and e_n is the LUE in the NPP calculation. Both e_g and e_n are usually estimated as a function of temperature, soil moisture and/or water vapor pressure deficit (VPD). In those PEM models, FAPAR has been estimated as a function of a greenness-related vegetation index, the Normalized Difference Vegetation Index (NDVI, Tucker, 1979):

$$\mathrm{NDVI} = \frac{\rho_{\mathrm{nir}} - \rho_{\mathrm{red}}}{\rho_{\mathrm{nir}} + \rho_{\mathrm{red}}} \quad (3)$$

where ρ_{red} and ρ_{nir} are reflectance values of red and near infrared (NIR) spectral bands. Monthly NDVI data from the NOAA Advanced Very High Resolution Radiometer (AVHRR) sensors that have only red and near infrared bands for the study of vegetation has been widely used in those PEM models (Prince & Goward, 1995).

Recently, we have developed a new satellite-based Vegetation Photosynthesis Model (VPM), which was first used to estimate GPP of an evergreen needleleaf forest from 1998 to 2001 at Howland, Maine, USA (Xiao et al., 2004). The VPM model takes advantages of additional spectral bands (e.g., blue and shortwave infrared (SWIR)) that are available from advanced optical sensors such as the VEGETATION (VGT) sensor onboard the SPOT-4 satellite, and the Moderate Resolution Imaging Spectroradiometer (MODIS) onboard the NASA Terra and Aqua satellites, which offer an improved potential for better characterization of vegetation at the global scale. The input data of the VPM model are the Enhanced Vegetation Index (EVI, Huete et al., 1997), Land Surface Water Index (LSWI, Xiao et al., 2004), air temperature and PAR. EVI is calculated, using reflectance data of blue, red and NIR bands:

$$\mathrm{EVI} = 2.5 \times \frac{\rho_{\mathrm{nir}} - \rho_{\mathrm{red}}}{\rho_{\mathrm{nir}} + (6 \times \rho_{\mathrm{red}} - 7.5 \times \rho_{\mathrm{blue}}) + 1} \quad (4)$$

LSWI is calculated as the normalized difference between NIR and SWIR spectral bands (Xiao et al., 2002):

$$\mathrm{LSWI} = \frac{\rho_{\mathrm{nir}} - \rho_{\mathrm{swir}}}{\rho_{\mathrm{nir}} + \rho_{\mathrm{swir}}} \quad (5)$$

For VGT images, we use NIR (0.78–0.89 μm) and SWIR (1.58–1.75 μm) bands. For MODIS images, we use NIR (841–875 nm) and SWIR (1628–1652 nm) bands.

In this study, we combined analysis of satellite images with CO_2 flux data from a temperate deciduous broadleaf forest site in Massachusetts, USA over the period of 1998–2001. The objective of this study was to develop and validate the satellite-based VPM (Xiao et al., 2004) for estimating seasonal dynamics of GPP of deciduous broadleaf forests. Simulations of VPM model were conducted, using 10-day VGT composite images over 1998–2001 and 8-day MODIS composite images in 2001, respectively. This study of multi-year satellite images and CO_2 flux data at Harvard Forest, Massachusetts, USA (Wofsy et al., 1993) will help us to address an important scaling-up question: to what degree can temporal dynamics (both seasonal and inter-annual) of GPP of deciduous broadleaf forests be observed and estimated from interpretations of remotely sensed images of advanced optical sensors combined with climate data. The VPM model uses improved vegetation indices derived from those advanced optical sensors and climate data (temperature and PAR), and may potentially provide more accurate estimates of GPP than other PEM models that employ NDVI only.

2. Brief description of satellite-based VPM

2.1. Overview of the VPM model

Leaf and forest canopies are composed of photosynthetically active vegetation (PAV, mostly chloroplast) and non-photosynthetic vegetation (NPV, mostly senescent foliage, branches and stems). The presence of NPV has a significant effect on FAPAR at the canopy level. For example, in forests with a leaf area index (LAI) of <3.0, NPV (stem) increased canopy FAPAR by 10–40% (Asner et al., 1998). Even within a green leaf, there is also some proportion of non-photosynthetic components (e.g., primary, secondary and tertiary veins, cell walls), dependent upon leaf type and leaf age. Non-photosynthetic absorption can vary in magnitude (e.g., 20–50%) depending on species, leaf morphology, leaf age and growth history (Hanan et al., 1998, 2002; Lambers

et al., 1998). Thus, FAPAR by a forest canopy should be partitioned into two components:

$$\mathrm{FAPAR} = \mathrm{FAPAR}_{\mathrm{PAV}} + \mathrm{FAPAR}_{\mathrm{NPV}} \quad (6)$$

where $\mathrm{FAPAR}_{\mathrm{PAV}}$ and $\mathrm{FAPAR}_{\mathrm{NPV}}$ represent the fraction of PAR absorbed by PAV and NPV, respectively. Only the PAR absorbed by PAV ($\mathrm{FAPAR}_{\mathrm{PAV}}$) is used for photosynthesis. Partitioning of FAPAR into $\mathrm{FAPAR}_{\mathrm{PAV}}$ and $\mathrm{FAPAR}_{\mathrm{NPV}}$ is a critical issue, but it has not been discussed extensively in the remote sensing community. Any model that accounts for $\mathrm{FAPAR}_{\mathrm{PAV}}$ is likely to substantially improve estimation of GPP or NPP of forests, given a known value of light use efficiency (LUE, g C/mol PAR or g C/MJ PAR) of forests.

Based on the conceptual partitioning of NPV and PAV within the leaf and canopy, we proposed a new satellite-based VPM for estimation of GPP over the photosynthetically active period of vegetation (Xiao et al., 2004):

$$\mathrm{GPP} = \varepsilon_g \times \mathrm{FAPAR}_{\mathrm{PAV}} \times \mathrm{PAR} \quad (7)$$

where PAR is the incident photosynthetically active radiation (μmol/m^2/s; photosynthetic photon flux density (PPFD)), and ε_g is the light use efficiency (μmol CO_2/μmol mol PPFD). Light use efficiency (ε_g) is affected by temperature, water and leaf phenology (leaf age):

$$\varepsilon_g = \varepsilon_0 \times T_{\mathrm{scalar}} \times W_{\mathrm{scalar}} \times P_{\mathrm{scalar}} \quad (8)$$

where ε_0 is the apparent quantum yield or maximum light use efficiency (μmol CO_2/μmol PPFD), and T_{scalar}, W_{scalar} and P_{scalar} are the downward-regulation scalars for the effects of temperature, water and leaf phenology (leaf age) on light use efficiency of vegetation, respectively.

T_{scalar} is estimated at each time step, using the equation developed for the Terrestrial Ecosystem Model (TEM) (Raich et al., 1991):

$$T_{\mathrm{scalar}} = \frac{(T - T_{\min})(T - T_{\max})}{[(T - T_{\min})(T - T_{\max})] - (T - T_{\mathrm{opt}})^2} \quad (9)$$

where $T_{\min}$, $T_{\max}$ and T_{opt} are minimum, maximum and optimal temperature for photosynthetic activities, respectively. If air temperature falls below $T_{\min}$, T_{scalar} is set to be zero.

The effect of water on plant photosynthesis (W_{scalar}) has been estimated as a function of soil moisture and/or water VPD in a number of PEM models (Field et al., 1995; Prince & Goward, 1995; Running et al., 2000). For instance, in the CASA (Carnegie, Stanford, Ames Approach) model, soil moisture was estimated using a one-layer bucket model (Malmstrom et al., 1997). Input data sets (e.g., precipitation, soil texture, soil depth) of soil moisture models usually have large spatial heterogeneity. Here, we explored an alternative approach that uses satellite-derived vegetation indices related to leaf and canopy water content. Availability of time series data of SWIR and NIR bands from the new generation of advanced optical sensors (e.g., VGT and MODIS) offers a new opportunity for quantifying leaf and canopy equivalent water content (EWT, g H_2O/m^2) at large spatial scales through both the vegetation indices approach (Ceccato et al., 2002a, 2002b) and the radiative transfer modeling approach (Zarco-Tejada et al., 2003). Four water-related vegetation indices that are based on NIR and SWIR bands have been developed: Moisture Stress Index (MSI, Hunt & Rock, 1989), Land Surface Water Index (LSWI, Xiao et al., 2002), Global Vegetation Moisture Index (GVMI, Ceccato et al., 2001, 2002a, 2002b) and Normalized Difference Water Index (NDWI, Gao, 1996). In this first version of the VPM model, as the first order of approximation, we proposed an alternative and simple approach that uses a water-sensitive vegetation index to estimate the seasonal dynamics of W_{scalar} (Xiao et al., 2004):

$$W_{\mathrm{scalar}} = \frac{1 + \mathrm{LSWI}}{1 + \mathrm{LSWI}_{\max}}. \quad (10)$$

where $\mathrm{LSWI}_{\max}$ is the maximum LSWI within the plant-growing season for individual pixels. LSWI values range from -1 to $+1$, and the simple formulation of W_{scalar} (Eq. (10)) is a linear scalar with a value range of 0 to 1.

Leaf age affects the seasonal patterns of photosynthetic capacity and net ecosystem exchange of carbon in a deciduous forest (Wilson et al., 2001). Results of a study that compared daily light use efficiency from four CO_2 flux tower sites (an agriculture field, a tallgrass prairie, a deciduous broadleaf forest and a boreal forest) support inclusion of parameters for cloudiness and the phenological status of the vegetation (Turner et al., 2003b). In the VPM model, P_{scalar} is included to account for the effect of leaf age on photosynthesis at the canopy level. In this version of the VPM model, calculation of P_{scalar} is dependent upon the longevity of leaves (deciduous versus evergreen). For a canopy that is dominated by leaves with a life expectancy of 1 year (one growing season, e.g., deciduous trees), P_{scalar} is calculated at two different phases as a linear function:

$$P_{\mathrm{scalar}} = \frac{1 + \mathrm{LSWI}}{2}$$

During bud burst to leaf full expansion (11)

$$P_{\mathrm{scalar}} = 1 \quad \text{After leaf full expansion} \quad (12)$$

The green-up phase (from bud burst to full leaf expansion) for temperate deciduous forests is short and usually last only for a few weeks. In our earlier studies for various vegetation types in Temperate East Asia (Boles et al., in press; Xiao et al., 2002), the results have indicated that the time series of greenness-related vegetation indices (e.g., NDVI, EVI) and water-related vegetation indices (LSWI) can be used to identify the green-up phase (from the

beginning of leaf-on to the completion of full leaf expansion) and senescence/leaf-off phase at the canopy level. LSWI values range from −1 to +1 (a range of 2), and the simplest formulation of P_{scalar} (Eq. (11)) is a linear scalar with a value range of 0 to 1.

To accurately estimate $FAPAR_{PAV}$ in forests is the most challenging task to the research communities of radiative transfer modeling and field measurements, as it is very difficult task to quantify PAV (g/m^2) and NPV (g/m^2) at the leaf and canopy levels. In this first version of the VPM model, $FAPAR_{PAV}$ within the photosynthetically active period of vegetation is estimated as a linear function of EVI (Xiao et al., 2004):

$$FAPAR_{PAV} = a \times EVI \quad (13)$$

At this first version of the VPM model, the coefficient a is set to be 1.0, representing the simplest case of parameterization. EVI is linearly correlated with the green LAI in crop fields, based on airborne multi-spectral data (Boegh et al., 2002). Evaluation of the radiometric and biophysical performance of EVI calculated from the MODIS sensor indicated that EVI remained sensitive to canopy variations (Huete et al., 2002). In an earlier study that compared VGT-derived NDVI and EVI for Northern Asia over the period of 1998–2001, the results indicated that EVI is less sensitive to residual atmospheric contamination due to aerosols from extensive fires in 1998 (Xiao et al., 2003).

2.2. Parameterization of the VPM model

In the VPM model, the maximum light use efficiency (ε_0) needs to be estimated for individual biomes. A literature survey was conducted to gather information on ε_0 for deciduous broadleaf forests. Here, we used $\varepsilon_0 = 0.044$ μmol mol CO_2/μmol PAR or $\varepsilon_0 = 0.528$ g C/mol PAR, based on an earlier study of CO_2 fluxes at Harvard Forest (Ruimy et al., 1995; Wofsy et al., 1993).

Estimation of site-specific $LSWI_{max}$ is dependent upon the optical sensor and the time series of image data. When multi-year LSWI data are available, the mean LSWI values of individual pixels over multiple years for individual temporal composite points (e.g., daily, weekly or every 10 days) were calculated, and then the maximum LSWI value within the photosynthetically active period was selected as an estimate of $LSWI_{max}$.

In calculation of T_{scalar}, T_{min}, T_{max} and T_{opt} values vary among different vegetation types (Aber & Federer, 1992; Raich et al., 1991). For temperate deciduous broadleaf forest, the PnET ecosystem model used 0, 20 and 40 °C for T_{min}, T_{opt} and T_{max}, respectively (Aber & Federer, 1992). The TEM used −2 °C for T_{min} of temperate forest (Raich et al., 1991). In this study, we used T_{min} of −1 °C, T_{opt} of 20 °C and T_{max} of 40 °C for temperate deciduous broadleaf forest.

3. The study site and data

3.1. Site-specific CO_2 flux and climate data from Harvard Forest

The eddy flux tower site (42.54°N and 72.18°W, 340 m elevation) is located within Harvard Forest, Petersham, MA, USA. Vegetation at the site is primarily a 60- to-80-year-old deciduous broadleaf forest, and dominant species composition include red oak (*Quercus rubra*), red maple (*Acer rubrum*), black birch (*Betula lenta*), white pine (*Pinus strobes*) and hemlock (*Tsuga canadensis*). Annual mean temperature is about 7.9 °C and annual precipitation is about 1066 mm. On the average, plant growing season lasts for 161 days (Waring et al., 1995).

Eddy flux measurements of CO_2, H_2O and energy at Harvard Forest have been collected since 1991 (Barford et al., 2001; Goulden et al., 1996; Wofsy et al., 1993). Daily data of maximum and minimum temperature (°C), precipitation (mm) and PAR (mol/m^2/day) from 1998 to 2001 were obtained from the website of Harvard Forest (http://www-as.harvard.edu/data/nigec-data.html). Daily measured NEE flux data and derived GPP and ecosystem respiration (R) at Harvard Forest from 1998 to 2001 were provided by researchers at Harvard Forest. Daily climate and CO_2 flux data were aggregated to the 10-day interval as defined by the 10-day composite VGT images (see Section 3.2) and the 8-day interval as defined by the 8-day composite MODIS images (see Section 3.3), respectively. For the VGT-based analysis, we calculated 10-day sums of PAR and CO_2 flux data, and 10-day means of air temperature. For the MODIS-based analysis, we calculated 8-day sums of PAR and CO_2 flux data, and 8-day means of air temperature.

We also obtained a LAI data set from the website of Harvard Forest (ftp://ftp.as.harvard.edu/pub/nigec/HU_Wofsy/hf_data/ecological_data/). This data set contains measurements of LAI taken in each of the 40 ecological monitoring plots during leaf out and leaf fall periods of 1998 (16 sampling dates) and 1999 (11 sampling dates). The LAI value for each plot is an average of five readings taken with a LICOR-2000 Plant Canopy Analyzer instrument, and calculated using the LICOR-2000 software. Here, we simply calculated the mean and standard deviation of LAI over the 40 plots for each sampling date. The fraction of photosynthetically active radiation absorbed by the vegetation canopy (FAPAR) was then calculated using the mean LAI values, light extinction coefficient ($k = 0.5$) and the equation (Ruimy et al., 1999):

$$FAPAR = 0.95(1 - e^{-k \times LAI}) \quad (14)$$

3.2. Ten-day composite images from VGT sensor

The VGT sensor onboard the SPOT-4 satellite has four spectral bands: blue (0.43–0.47 μm), red (0.61–0.68 μm),

NIR (0.78–0.89 μm) and SWIR (1.58–1.75 μm). The VGT sensor provides daily global images at 1-km spatial resolution. The standard 10-day composite data (VGT-S10) are produced and freely available to the public (http://www.free.vgt.vito.be). The temporal compositing method for generating standard 10-day synthetic products (VGT-S10) is to select an observation with the maximum NDVI value within a 10-day period. There are three 10-day composites within a month: days 1–10, days 11–20 and day 21 to the end of the month.

We acquired the VGT-S10 data (http://www.free.vgt.vito.be) over the period from April 1–10, 1998 to December 21–31, 2001 for the globe (a time series data of 135 VGT-S10 images). Vegetation indices (NDVI, EVI, LSWI) were calculated for all the 10-day composite images (VGT-S10). A detailed description of the pre-processing and calculation of vegetation indices from VGT-S10 data were given elsewhere (Xiao et al., 2003). For a time series of vegetation index, we used a simple gap filling method (Xiao et al., 2003) to fill vegetation index values of those cloudy pixels identified by the quality flag in the VGT-S10 reflectance files. We first selected a three-point time series filter, $X(t-1)$, $X(t)$ and $X(t+1)$ and used values of non-cloudy pixels in this window to correct cloudy pixel. If both $X(t-1)$ and $X(t+1)$ pixels were cloud-free, we calculated the average of $X(t-1)$ and $X(t+1)$, and used the average value to replace $X(t)$. If only one pixel (either $X(t-1)$ or $X(t+1)$) was cloud-free, we used that pixel to replace $X(t)$. If the algorithm did not succeed in a three-point time series filter, we then extended to a five-point time series filter, $X(t-2)$, $X(t-1)$, $X(t)$, $X(t+1)$, $X(t+2)$, using the same procedure as the above three-point time series filter.

In this study, we extracted spectral bands and vegetation indices data for one 1-km pixel that covers the eddy flux tower site at Harvard Forest. We recognized the geo-location error of optical sensors (both VGT and MODIS sensors), which becomes larger when the sensor is off-nadir. The conventional approach is to calculate the average of an $N \times N$ pixel block (e.g., N is often set to be 3 or 5 pixels, or large number), and to use the averaged values in model simulations and compare simulation results with the ground truth data. Note that the footprint size of the forest flux tower site is often at a few hundreds of meters to 1 km, although it varies substantially dependent upon the height of flux tower, wind direction, speed, topography, etc. The average of an $N \times N$ pixel block may generate representation of a "pseudo pixel" that is not consistent (often too large) in spatial domain with the tower footprint, and the problem could become worse in the landscape of complex topography. As our long-term goal is to generate global GPP estimates at the original image spatial resolution (e.g., 1 km for VGT sensor and 500 m for MODIS sensor), we are interested in the performance of the VPM model at the single pixel level. Therefore, in this study, we reported data analyses and simulation results for a single image pixel (for both VGT and MODIS images), instead of an $N \times N$ pixel block.

3.3. Eight-day composite images from MODIS sensor

The MODIS sensor onboard the NASA Terra satellite was launched in December 1999. Of the 36 spectral bands in the MODIS sensor, seven spectral bands are primarily designed for the study of vegetation and land surface: blue (459–479 nm), green (545–565 nm), red (620–670 nm), near infrared (841–875 nm, 1230–1250 nm) and shortwave infrared (1628–1652 nm, 2105–2155 nm). The MODIS sensor acquires daily images of the globe at a spatial resolution of 250 m for red and near infrared (841–875 nm) bands, and at a spatial resolution of 500 m for blue, green, near infrared (1230–1250 nm) and shortwave infrared bands. The MODIS Land Science Team provides a suite of 8-day composite products to the users (http://www.modis-land.gsfc.nasa.gov/), including the 8-day Surface Reflectance product (MOD09A1) that has the above seven spectral bands, and the 8-day Lear Area Index and Fraction of Photosynthetically Active Radiation absorbed by the Vegetation Canopy (LAI/FPAR product, MOD15A2). The LAI/FPAR products were derived from the LAI/FPAR algorithms described by Knyazikhin et al. (1998). Both the MODIS surface reflectance and LAI/FPAR data sets have a spatial resolution of 500 m and are provided to users in a tile fashion (each tile covers 10° latitude by 10° longitude).

We downloaded the 8-day Surface Reflectance (MOD09-A1) and the 8-day LAI/FPAR data sets for the period of 1/2001–12/2002 from the EROS Data Center, US Geological Survey (http://www.edc.usgs.gov/). Note that there were no MODIS data acquisitions during June 10 to July 3, 2001 because the MODIS sensor experienced technical failure. Reflectance values of the 8-day surface reflectance data set from these four spectral bands (blue, red, near infrared (841–875 nm), shortwave infrared (1628–1652 nm)) were used to calculate vegetation indices (NDVI, EVI and LSWI). The procedure employed for gap filling of cloudy pixels in the time series of vegetation indices was the same as that used for the VEGETATION data set (see Section 3.2).

Based on the geo-location information (latitude and longitude) of the CO_2 flux tower site at Harvard Forest, data of vegetation indices and FAPAR were extracted from one MODIS pixel that is centered on the flux tower. We included the MODIS data in 2002 in this study to check whether the seasonal patterns of vegetation indices are consistent in 2001 and 2002. Because CO_2 flux data in 2002 are not available for this study, simulations of the VPM model are driven by MODIS images in 2001.

3.4. Simulations of the VPM model

Two simulations of the VPM model were conducted in an effort to evaluate the potential of VGT and MODIS sensors. First, we ran the VPM model using multi-year vegetation indices (EVI, LSWI) derived from 10-day VGT composites, site-specific air temperature and PAR data in 4/1998–12/

2001. Secondly, we conducted a simulation of the VPM model using vegetation indices (EVI, LSWI) derived from the 8-day MODIS surface reflectance product, site-specific air temperature and PAR data from the tower site in 2001. In both simulations, the VPM-predicted GPP values were compared with observed GPP data at the flux tower site.

4. Results

4.1. Temporal analyses of CO_2 fluxes and VGT data in 1998–2001

The NEE and GPP time series during 1998–2001 at Harvard Forest had a distinct seasonal cycle (Fig. 1a). GPP values were near zero in winter season (December, January, February), because the deciduous dominated canopy is bare and low air temperature and frozen soil inhibit photosynthetic activities of conifer trees (Fig. 1a). GPP began to increase in late March and reached its peak in late June to early July. GPP declined rapidly after its peak, despite the fact that LAI changed little over the period between July and September (Fig. 2a). The seasonal dynamics of GPP can be explained in part by the seasonal dynamics of air temperature and PAR (Fig. 1b).

The comparisons between vegetation indices (EVI, NDVI) and GPP have shown that the seasonal dynamics of EVI better mimic those of GPP in terms of phase and amplitude (Fig. 3). EVI curves had a peak value in early July, while NDVI curves had a plateau from July to September. When using all the observations in 1998–2001 (Fig. 3), EVI had a stronger linear relationship with GPP than NDVI (Fig. 4). The relationship between EVI and GPP indirectly supports our hypothesis that $FAPAR_{PAV}$

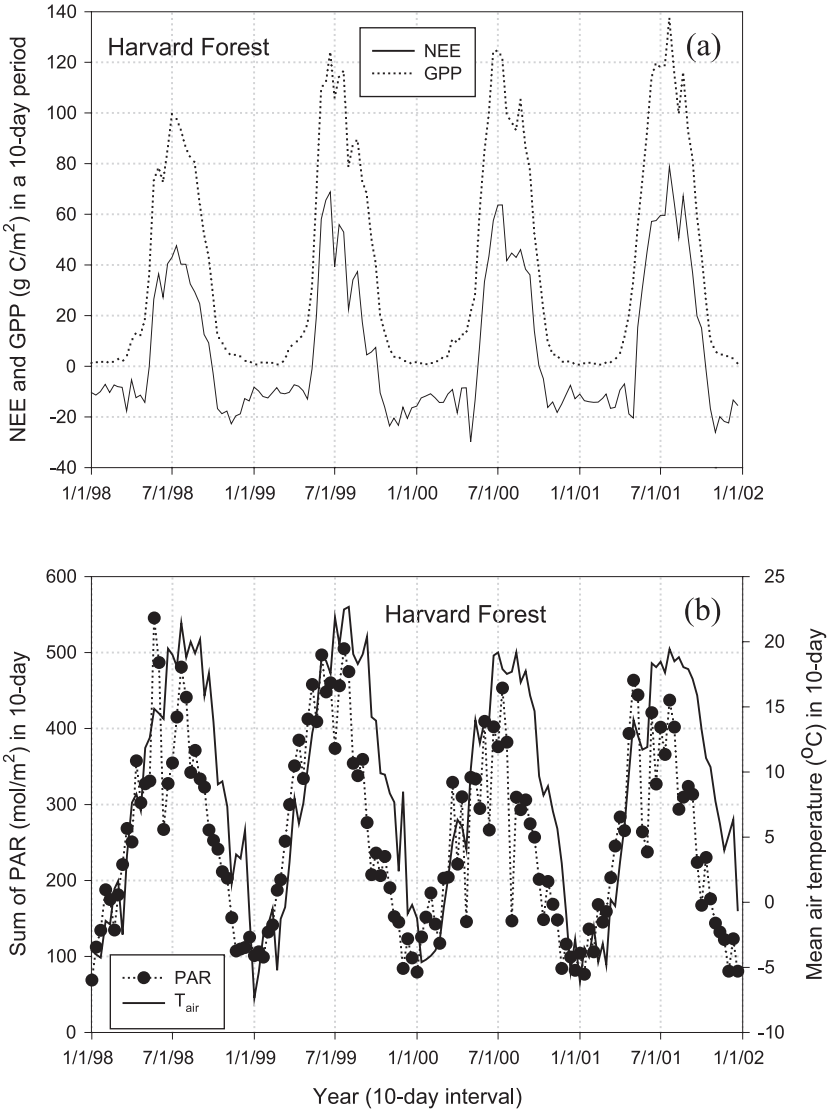

Fig. 1. The seasonal dynamics of net ecosystem exchange of CO_2 (NEE), gross primary production (GPP), photosynthetically active radiation (PAR) and mean air temperature from 1998 to 2001 for the deciduous broadleaf forest at Harvard Forest, Massachusetts.

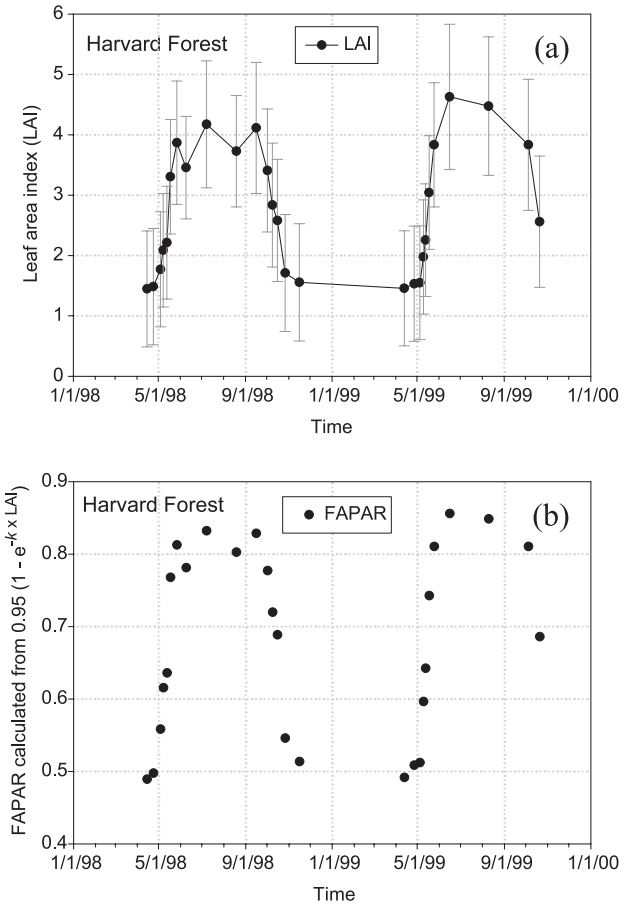

Fig. 2. The seasonal dynamics of leaf area index (LAI) and fraction of photosynthetically active radiation absorbed by the vegetation canopy (FAPAR) in 1998–1999 at Harvard Forest, Massachusetts.

during the plant growing season can be estimated by an improved vegetation index (e.g., EVI in this study).

The time series of LSWI data have a distinct seasonal cycle with a spring trough and a fall trough (Fig. 5). The high LSWI values in late fall, winter and early spring are attributed to snow cover (above or below the canopy). The green-up period for the calculation of P_{scalar} is defined as the period from the date that had the minimum LSWI in spring to the date that had the maximum LSWI in early summer. We calculated the means of LSWI for each of the 10-day periods over the 4-year (1998–2001) data (Fig. 5), and the maximum LSWI ($LSWI_{max} = 0.40$, in June 1–10) within April–June (the green-up period) was selected as an estimate of $LSWI_{max}$ and used in the calculation of W_{scalar}.

At a temporal resolution of 10 days, the predicted GPP (GPP_{pred}) from the VPM model agreed reasonably well with observed GPP (GPP_{obs}) data from 1998 to 2001 (Figs. 6 and 7). The seasonal dynamics of GPP_{pred} were similar to those of GPP_{obs} in terms of phase and magnitude (Fig. 6). Seasonally integrated GPP_{obs} over the period of April 1 to November 30 accounted for 98% of annual GPP_{obs} (Table 1). In comparison to the seasonally integrated GPP_{obs} values, seasonally integrated GPP_{pred} was +11% (in 1998), +9% (in 1999), −16% (in 2000) and −9% (in 2001), respectively (Table 1).

4.2. Temporal analyses of CO_2 flux and MODIS data in 2001–2002

The NDVI curve derived from the standard 8-day MODIS surface reflectance products in 2001–2002 had a

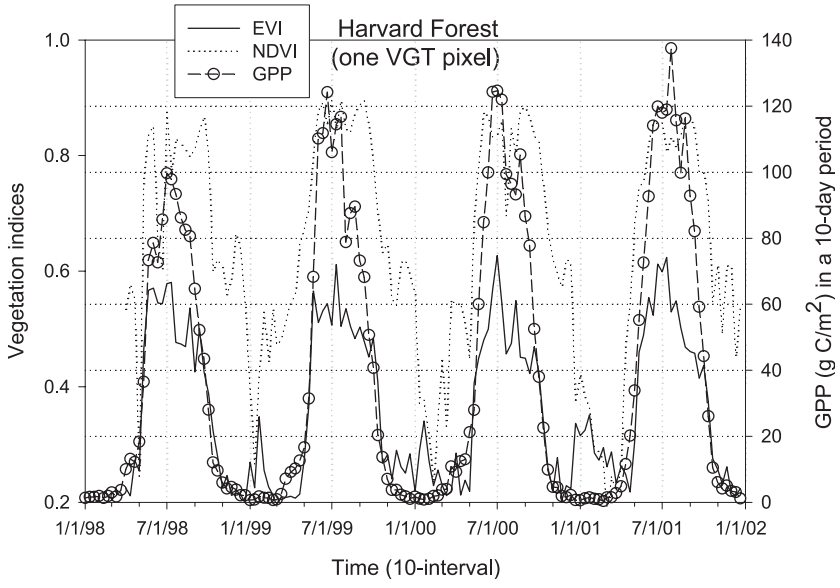

Fig. 3. The seasonal dynamics of gross primary production (GPP), Enhanced Vegetation Index (EVI) and Normalized Difference Vegetation Index (NDVI) during 1998–2001 at Harvard Forest, Massachusetts.

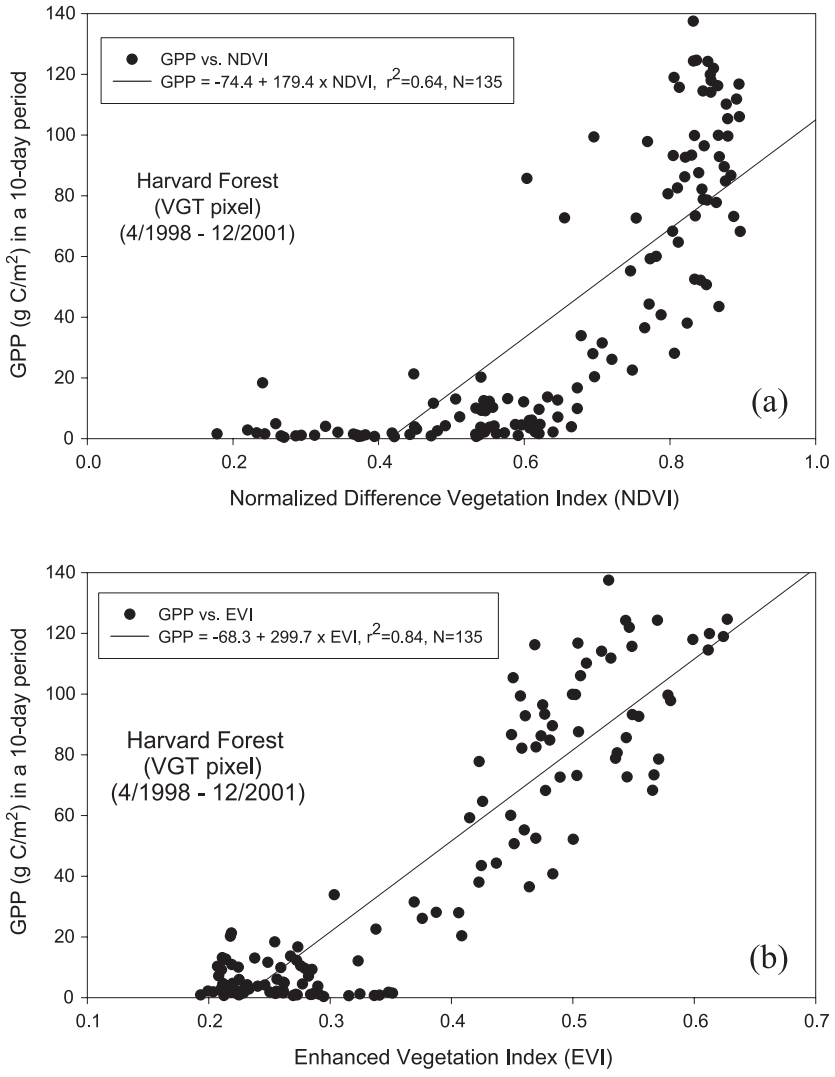

Fig. 4. Simple linear regression analyses between gross primary production (GPP) of forest and vegetation indices (NDVI, EVI) during 4/1998–12/2001 at Harvard Forest, Massachusetts.

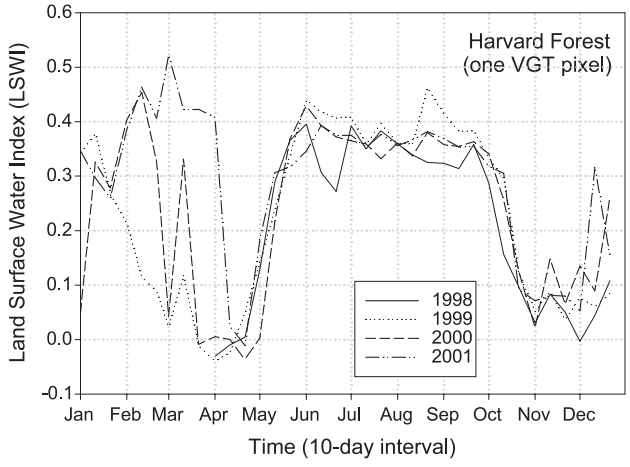

Fig. 5. The seasonal dynamics of VGT-derived Land Surface Water Index (LSWI) in 4/1998–12/2001 at Harvard Forest, Massachusetts.

distinct seasonal cycle, with a plateau in summer (Fig. 8). The FAPAR curve from the standard LAI/FPAR product had very similar seasonal dynamics to the NDVI curve. Because no field-measured LAI data in 2001 and 2002 are available for this study, we used field-measured LAI data in 1998–1999 (Fig. 2a) to calculate FAPAR (see Eq. (14)). Based on the field measured LAI data in 1998–1999 (Fig. 2a), FAPAR had a maximum value of 0.83 in 1998 and 0.85 in 1999 (Fig. 2b). No major disturbance took place between 1998 and 2002 at the Harvard Forest, therefore, the MODIS-based FAPAR in the plant growing season seems to agree reasonably well with the LAI-based FAPAR in terms of phase and magnitude (Figs. 2b and 8).

The EVI curve differs substantially from the NDVI and FAPAR curves, and has a distinct seasonal dynamics with a peak value in late June to early July over 2001–2002 (Fig. 8). In June 2–9, 2001, the EVI value was 0.66 and the FAPAR value was 0.89 (Fig. 8). As we hypothesize that EVI

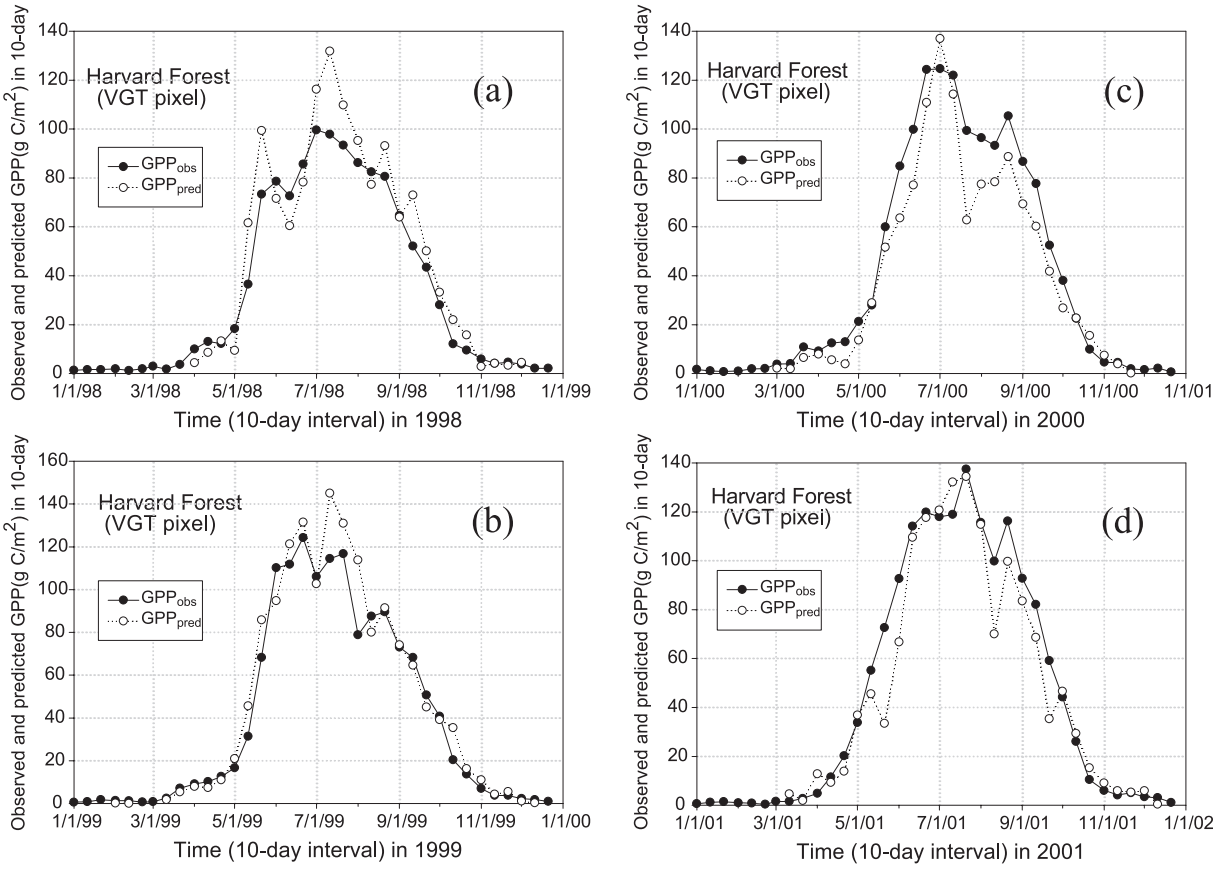

Fig. 6. The seasonal dynamics of predicted gross primary production (GPP) from the VPM model and observed GPP at Harvard Forest during 4/1998–12/2001. Vegetation indices (EVI, LSWI) derived from the 10-day VGT composite images (VGT-S10), site-specific air temperature and PAR data were used in simulation of the VPM model.

approximates $FAPAR_{PAV}$ and $FAPAR_{NPV}$ is calculated as the difference between FAPAR and EVI, the $FAPAR_{NPV}$ in June 2–9, 2001 was estimated to be 0.23 (0.89–0.66 = 0.23), accounting for ~26% of the total FAPAR (=(0.89 − 0.66)/0.89). In 2001, the observed GPP increased gradually from April and reached its peak value in late June (Fig. 9a). The seasonal dynamics of GPP in 2001 can be partially explained by the seasonal dynamics of temperature and PAR (Fig. 9b). The observed GPP in 2001 had similar seasonal dynamics with EVI in the plant growing season, with a peak value in an 8-day period of late June (Fig. 9a). The EVI time series data had a stronger linear relationship with observed GPP than did the NDVI time series in 2001 (Fig. 10). High EVI and LSWI values in late fall, winter and early spring are attributed to snow cover. The time series of LSWI data also had a spring trough and a fall trough in 2001 (Fig. 9a). The maximum LSWI ($LSWI_{max}$ = 0.43, in June 2–9, 2001) during the green-up period (April–June) of 2001 was selected as an estimate of $LSWI_{max}$ (Fig. 9a) and then used in calculation of W_{scalar}.

Simulation of the VPM model was run using vegetation indices (EVI, LSWI) derived from the 8-day MODIS Surface Reflectance Product, site-specific air temperature and PAR data in 2001. The seasonal dynamics of predicted GPP in 2001 agreed reasonably well the observed GPP in terms of phase and magnitude (Fig. 11a). The simple linear regression model also shows high correlation between predicted GPP and observed GPP in 2001 (Fig. 11b).

5. Discussions and summary

As the leaf phenological cycle (leaf flush, expansion, senescence, fall) progresses, leaves of the deciduous forest canopy change in their biophysical (e.g., leaf structure and thickness), biochemical (e.g., chlorophyll and other pigments, nitrogen) and optical properties, which in turn influence both biophysical parameters (e.g., albedo, latent and sensible heat flux) and biogeochemical parameters (e.g., photosynthesis) of the land surface. Limited studies had evaluated radiometric and biophysical performance of vegetation indices (EVI, NDVI) from MODIS data (Huete et al., 2002) and for VGT data (Xiao et al., 2003, 2004). In this study, we evaluated the biophysical performance of vegetation indices (NDVI and EVI) in relation to GPP of a deciduous broadleaf forest. The quantitative relationships between the vegetation indices (EVI and NDVI) and CO_2 flux data clearly demonstrated the improvement of EVI over

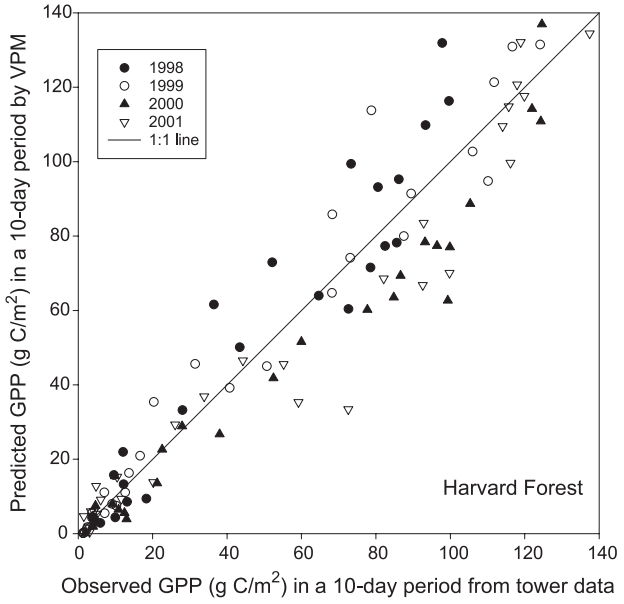

Fig. 7. A simple linear regression analysis between predicted gross primary production (GPP) from the VPM model and observed GPP at Harvard Forest during 4/1998–12/2001. Vegetation indices (EVI, LSWI) from the 10-day VGT composites, site-specific air temperature and PAR data were used in simulation of VPM model. A total of 110 GPP_{pred} values in 4/1998–12/2001 were used in the simple linear regression analysis: $GPP_{pred} = 0.97 \times GPP_{obs}$, $r^2 = 0.92$, $N = 110$, $p < 0.0001$.

NDVI, in terms of the phase and magnitude of photosynthesis of deciduous broadleaf forests. Time series of EVI and LSWI may provide valuable insight into the processes (e.g., growing season length and water stress) that regulate forest carbon exchange. NEE during the 1998 and 2001 growing seasons were extremes among the multi-year (1991–2002) NEE data from the flux tower site at Harvard Forest. Net uptake of CO_2 was about 1/3 below and 1/2 above the long term mean in 1998 and 2001, respectively, and was driven by anomalous GPP in both years (Urbanski, unpublished data). In 1998, low LSWI in the late summer indicates some degree of water stress (Fig. 5), and the rapid October decline of both EVI and LSWI indicates an early senescence of leaves (Figs. 3 and 5). High EVI and LSWI in May of 2001 indicate a rapidly developing and photosynthetically active canopy, and high LSWI in mid-October of 2001 indicates a late senescence of leaves. The integrated EVI over the summer months (June–August) of 2001 is the highest of the four years (1998–2001). The observed differences between the improved vegetation indices (EVI and LSWI) and NDVI clearly highlights the needs for radiative transfer modeling and seasonal-long field measurements of biophysical, biochemical and optical properties at the leaf and canopy levels, which would lead to improving our understanding of the seasonal dynamics and biophysical performance of improved vegetation indices (e.g., EVI, LSWI in this study) for deciduous broadleaf forests.

In addition to EVI, a set of the "Advanced Vegetation Indices" that are optimized for the retrieval of FAPAR from individual optical sensors have been developed (Gobron et al., 1999, 2000; Govaerts et al., 1999). Detailed information on mathematical formulae and parameters of these advanced vegetation indices was given elsewhere (Gobron et al., 2000). The implementation of these vegetation indices requires the Top-of-Atmosphere (TOA) bidirectional reflectance factors (BRFs) data as input data, and blue band is used to rectify red and NIR bands (Gobron et al., 2000). These sensor-specific advanced vegetation indices have been optimized for the Medium Resolution Imaging Spectrometer (MERIS), the Global Imager (GLI) and the VEGETATION sensors. Clearly, there is a need to examine those advanced vegetation indices in relation to leaf phenology and the seasonal dynamics of GPP across the flux tower sites in various biomes.

The simulation results of the VPM model have shown that predicted GPP agreed well with observed GPP of a temperate deciduous broadleaf forest at the Harvard Forest. The results from this study of deciduous broadleaf forest and an earlier study of evergreen needleleaf forest (Xiao et al., 2004) indirectly support the PAV–$FAPAR_{PAV}$–EVI hypotheses and leaf water–LSWI hypothesis implemented in the VPM model. Recently, the standard MODIS-based GPP estimates (8-day composite) from the MODIS-PSN algorithm that uses FAPAR and water vapor pressure deficit (Running et al., 1999) become available to the public. The standard GPP products (MOD17A2, Collection 4) of 2001 (tile H12V04, covering the Harvard Forest) were downloaded from the EROS Data Center, US Geological Survey (http://www.edc.usgs.gov). The comparison between predicted GPP from the MODIS-PSN algorithm with observed GPP from the CO_2 eddy flux tower in the Harvard Forest clearly shows the MODIS-PSN algorithm does not work well for the deciduous broadleaf forest (Fig. 12). The MODIS-PSN algorithm over-estimated GPP in the early part (April) of the plant growing season and under-estimated GPP from June to September. The similar situation was also reported in another study that used the MODIS-PSN algorithm for the Harvard Forest site (Turner et al., 2003a). That

Table 1
Annual gross primary production (g C/m^2, from January 1 to December 31, GPP_{1-12}) and seasonally integrated sums (April 1 to November 30) of gross primary production (GPP_{4-11}), photosynthetically active radiation (PAR_{4-11}, mol/m^2) and precipitation (PPT_{4-11}, mm) at Harvard Forest, Massachusetts

Year	Tower site data[a]		VPM model	NPP[b]	Site information	
	GPP_{1-12}	GPP_{4-11}	$GPP_{pred(4-11)}$	$NPP_{pred(4-11)}$	PAR_{4-11}	PPT_{4-11}
1998	1191	1164	1298	610	7257	581
1999	1391	1369	1486	698	7963	647
2000	1424	1392	1169	549	6727	731
2001	1580	1561	1416	656	7659	520
Mean	1397	1372	1342	628	7402	620

[a] Tower site data — based on daily GPP data at the flux tower.
[b] NPP (g C/m^2)—based on the NPP/GPP ratio = 0.47 (Waring et al., 1998), $NPP_{pred(4-11)} = 0.47 * GPP_{pred(4-11)}$.

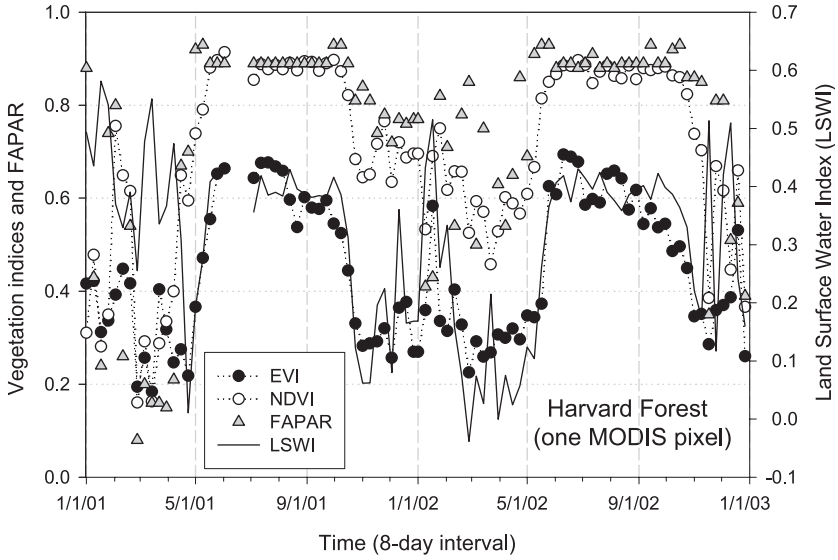

Fig. 8. The seasonal dynamics of vegetation indices (EVI, NDVI, LSWI) derived from the 8-day MODIS Surface Reflectance Product (MOD09A1) and FAPAR from the 8-day MODIS Leaf Area Index and Fraction of Photosynthetically Active Radiation Absorbed by the Vegetation Canopy Product (LAI/FPAR Product, MOD15A2) in 2001–2002 at Harvard Forest, Massachusetts. EVI—Enhanced Vegetation Index; NDVI—Normalized Difference Vegetation Index; LSWI—Land Surface Water Index.

study also reported that the site-specific daily minimum temperature and vapor pressure deficit are highly correlated to those from the NASA Data Assimilation Office (DAO) at the coarse spatial resolution, and site-specific daily PAR is slightly lower than PAR from the DAO at the coarse spatial resolution (Turner et al., 2003a). Therefore, the large discrepancies between predicted GPP from the MODIS-PSN algorithm and observed GPP from the flux tower (see Fig. 12 and Turner et al., 2003a) are not likely to be explained by climate input data (site specific data versus the DAO data). Similar to the other PEMs (Behrenfeld et al., 2001; Field et al., 1998; Potter et al., 1993; Prince & Goward, 1995), the MODIS-PSN algorithm (Running et al., 1999; Turner et al., 2003a) is built upon the LAI–FAPAR–NDVI relationships. As the VPM model is built upon the PAV–$FAPAR_{PAV}$–EVI hypotheses, a comparison between the VPM model and the MODIS-PSN and other PEMs across many CO_2 eddy flux tower sites is needed in the future.

Among simulation results of the VPM model, there were large differences between GPP_{pred} and GPP_{obs} for a few 10-day periods (Fig. 6), accounting for most of the differences between seasonally integrated GPP_{obs} and GPP_{pred} (Table 1). The large discrepancy between GPP_{obs} and GPP_{pred} in those 10-day periods can be attributed in part to prediction error of GPP_{pred} from the VPM model and in part to estimation error of GPP_{obs}. One factor that affects GPP predictions of the VPM model is the vegetation indices from 10-day composite images. The compositing method (currently selecting an observation with the maximum NDVI value in a 10-day period) could result in some bias, and one resolution to the issue would be to use daily images as input to the VPM model, although this would requires substantial increases in computer processing. In some case, under-estimation of GPP from the VPM model is attributed to lower input PAR values. For instance, the PAR value in July 21–31, 2000 was low, because of frequent cloud cover as indicated by a large amount of precipitation in that 10-day period, and the VPM model predicted a lower GPP value (Fig. 6). For applications of the VPM model at large spatial scales, PAR is the most critical variable in the estimation of the seasonal dynamics of GPP_{pred}, but it varies substantially over space and time. Therefore, improvement in measurement of PAR (both direct and diffusive) at large spatial scale would substantially benefit the VPM and other models that estimate GPP of terrestrial ecosystems. The estimation error (either overestimation or underestimation) of GPP_{obs} at the daily time scale should also be considered. GPP_{obs} is calculated from field-measured NEE (NEE_{obs}) and ecosystem respiration (R_{day} and R_{night}): $NEE_{obs} = GPP_{obs} - (R_{day} + R_{night})$. While night-time NEE is equivalent to night-time ecosystem respiration (R_{night}), there is large uncertainty in estimating daytime ecosystem respiration (R_{day}). For a given value of NEE as measured by the eddy-covariance method, an error in the estimation of R_{day} would result in an error in the estimation of GPP. The two major steps that must be taken to derive daily GPP are the gap filling of both NEE and R_{day}. Both of these steps require subjective decisions and are currently the subject of a great deal of discussion (Falge et al., 2001). Note that there is no objective data set available to validate GPP estimates from the various methods of gap filling of NEE and R_{day}. The daily GPP data we used in this study represent the average values of daily GPP from three different gap filling methods.

Calculation of GPP is the first step in the study of the carbon cycle of terrestrial ecosystems. Estimation of an-

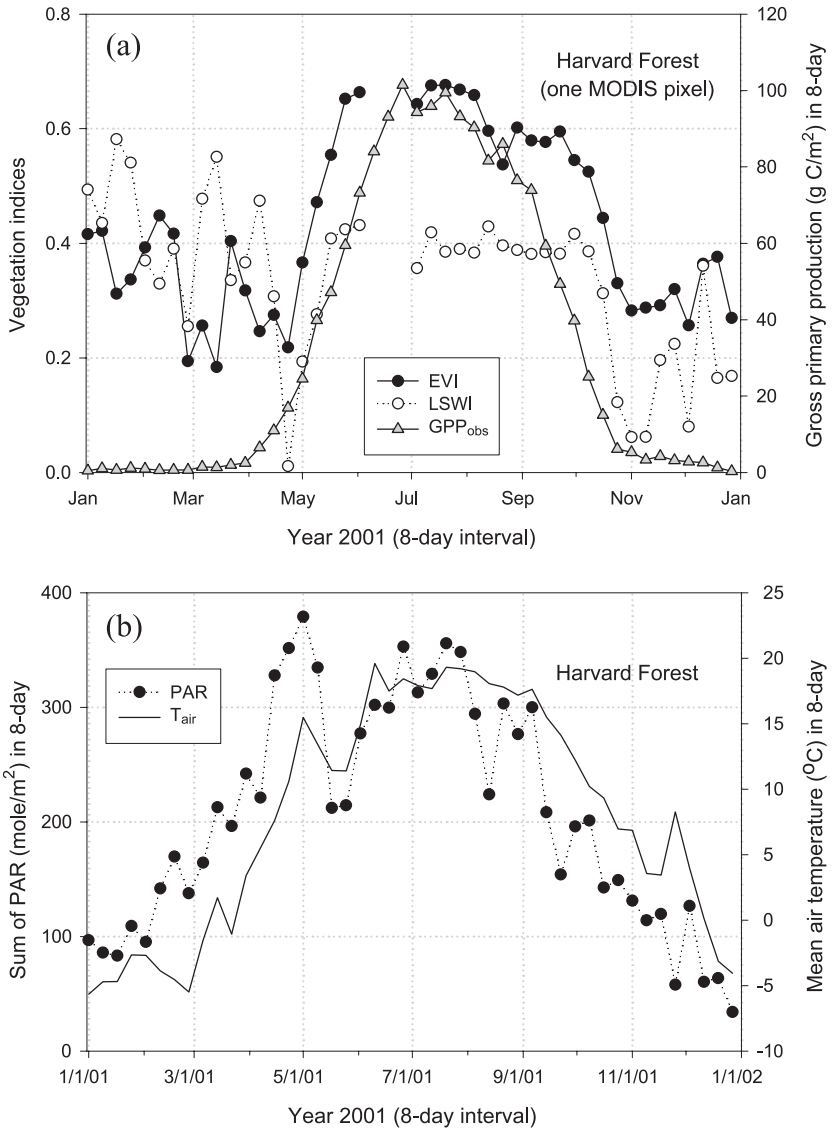

Fig. 9. The seasonal dynamics of vegetation indices (EVI, LSWI) derived from the 8-day MODIS Surface Reflectance Product (MOD09A1), observed gross primary production (GPP_{obs}), air temperature (T_{air}) and photosynthetically active radiation (PAR) in 2001 at Harvard Forest, Massachusetts. EVI—Enhanced Vegetation Index; LSWI—Land Surface Water Index.

nual NPP of terrestrial ecosystems, which is defined as the difference between GPP and autotrophic respiration of vegetation, is also needed. Annual carbon budgets were assembled for six evergreen forests and one deciduous forest in Oregon, USA, three pine plantations in New South Wales, Australia, a deciduous forest in Massachusetts, and a *Nothofagus* forest on the South Island of New Zealand (Waring et al., 1998). The comparative analysis indicated that the total NPP/GPP ratio was conservative (0.47 ± 0.04 S.D.). In this study, we used the invariant NPP/GPP ratio to estimate annual NPP of deciduous broadleaf forest at Harvard Forest. Using the seasonally integrated GPP_{pred} from April 1 to November 30, seasonally integrated NPP ranges from 549 g C/m^2 in 2000 to 698 g C/m^2 in 1999, with a 4-year mean of 628 g C/m^2 (Table 1). Based on the field data at Harvard Forest (Aber et al., 1993; Williams et al., 1997), Waring et al. (1998) reported an aboveground NPP of 457 g C/m^2/year and a belowground NPP of 202 g C/m^2/year, resulting in an annual NPP of 659 g C/m^2/year, which is within the range of annual NPP estimates from 1998 to 2001 from the VPM model (Table 1).

In summary, this study has clearly shown that the improved vegetation indices (EVI, LSWI) from the VGT and MODIS sensors provide far more information on the seasonal dynamics of deciduous broadleaf forest at the leaf and canopy levels than NDVI and FAPAR. This study has also demonstrated that the potential of the VPM model for quantifying the seasonal dynamics and interannual variations of GPP of deciduous broadleaf forest, using improved vegetation indices (EVI, LSWI) from the VGT and MODIS sensors. At present, over 200 CO_2 eddy flux

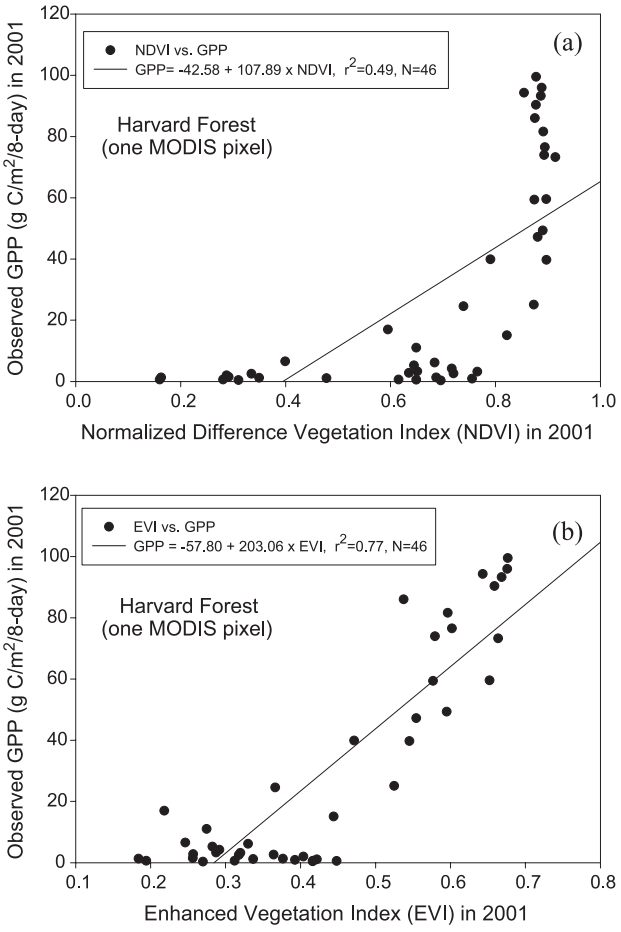

Fig. 10. The simple linear regression analyses between observed gross primary production and vegetation indices (EVI, NDVI) derived from the 8-day MODIS Surface Reflectance Product (MOD09A1) in 2001 at Harvard Forest, Massachusetts.

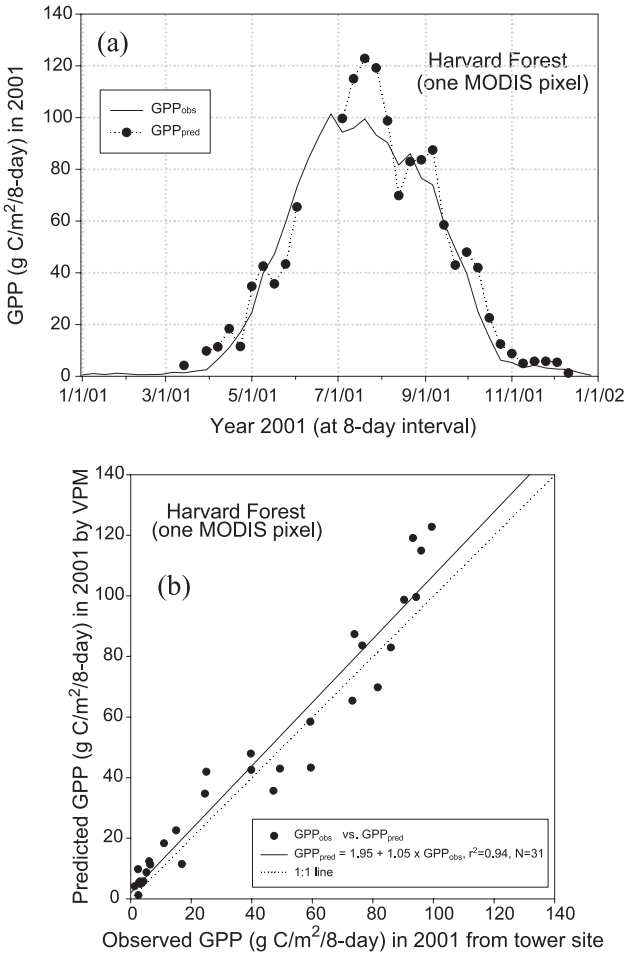

Fig. 11. A comparison between the predicted and observed gross primary production (GPP) in 2001 at Harvard Forest, Massachusetts. Vegetation indices derived from the 8-day MODIS Surface Reflectance Product (MOD09A1), and site-specific air temperature and PAR data were used in simulation of the VPM model.

tower sites in the world constitute a global FLUXNET network (http://www.daac.ornl.gov/FLUXNET/fluxnet.html). Abundant data of CO_2, H_2O and energy flux for a variety of ecosystem types have been accumulated. Data on site vegetation, soil, hydrologic and meteorological characterization at the tower sites have also been collected. Multi-year GPP data from those eddy flux tower sites can be used to validate the VPM model. The availability of those data from the flux tower sites will take some time, because analysis and publication of those flux data are time consuming. Once data from most flux tower sites become available to the public in the near future, a mega-data analysis of CO_2 fluxes, climate and vegetation indices across various ecosystem types will help quantify the uncertainty of the VPM model, including the maximum light use efficiency (ε_0) across various vegetation types (Ruimy et al., 1995). With further validation and development, the VPM model has the potential to be applied at large spatial scales to estimate GPP of forests, which would improve our understanding of the carbon cycle of the terrestrial biosphere.

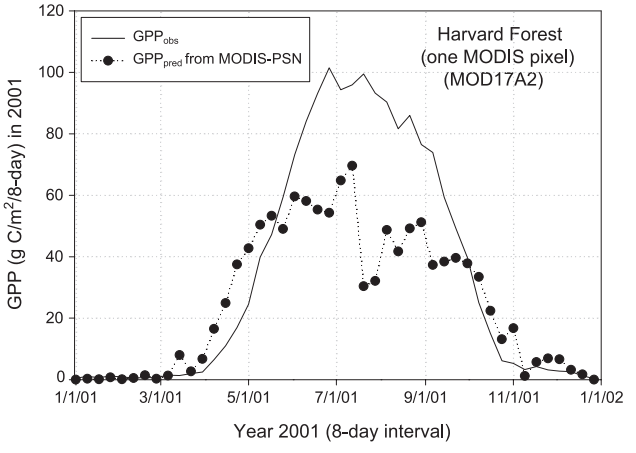

Fig. 12. A comparison between predicted gross primary production (GPP) from the standard MODIS GPP/NPP product (MOD17A2) and observed GPP from the flux tower site in 2001 at Harvard Forest, Massachusetts. The MODIS-PSN algorithm (Running et al., 1999; Turner et al., 2003a) is used to generate the standard MODIS GPP/NPP product (MOD17A2), which is now available to the public (http://www.edc.usgs.gov).

Acknowledgements

We thank the researchers who worked at the eddy flux tower of Harvard Forest for providing multi-year CO_2 flux, climate and leaf area index data. The analyses of vegetation indices and simulations of the VPM model were supported by research grants from NASA Interdisciplinary Science Program (NAG5-10135) and Land Cover and Land Use Change Program (NAG5-11160). Field activities at the Harvard Forest tower site were supported by the Department of Energy and NASA.

References

Aber, J. D., & Federer, C. A. (1992). A generalized, lumped-parameter model of photosynthesis, evapotranspiration and net primary production in temperate and boreal forest ecosystems. *Oecologia*, *92*, 463–474.

Aber, J. D., Magill, A., Boone, M., Melillo, J. M., Steudler, P. A., & Bowden, R. D. (1993). Plant and soil responses to chronic nitrogen additions at the Harvard Forest, Massachusetts. *Ecological Applications*, *3*, 156–166.

Asner, G. P., Wessman, C. A., & Archer, S. (1998). Scale dependence of absorption of photosynthetically active radiation in terrestrial ecosystems. *Ecological Applications*, *8*, 1003–1021.

Barford, C. C., Wofsy, S. C., Goulden, M. L., Munger, J. W., Pyle, E. H., Urbanski, S. P., Hutyra, L., Saleska, S. R., Fitzjarrald, D., & Moore, K. (2001). Factors controlling long- and short-term sequestration of atmospheric CO2 in a mid-latitude forest. *Science*, *294*, 1688–1691.

Behrenfeld, M. J., Randerson, J. T., McClain, C. R., Feldman, G. C., Los, S. O., Tucker, C. J., Falkowski, P. G., Field, C. B., Frouin, R., Esaias, W. E., Kolber, D. D., & Pollack, N. H. (2001). Biospheric primary production during an ENSO transition. *Science*, *291*, 2594–2597.

Boegh, E., Soegaard, H., Broge, N., Hasager, C. B., Jensen, N. O., Schelde, A., & Thomsen, A. (2002). Airborne multispectral data for quantifying leaf area index, nitrogen concentration, and photosynthetic efficiency in agriculture. *Remote Sensing of Environment*, *81*, 179–193.

Boles, S., Xiao, X., Liu, J., Zhang, Q., Munkhutya, S., Chen, S., & Ojima, D. (2004). Land cover characterization of temperate East Asia: Using multi-temporal image data of VEGETATION sensor. *Remote Sensing of Environment, 90*(4), 477–489.

Ceccato, P., Flasse, S., & Gregoire, J. M. (2002a). Designing a spectral index to estimate vegetation water content from remote sensing data: Part 2. Validation and applications. *Remote Sensing of Environment*, *82*, 198–207.

Ceccato, P., Flasse, S., Tarantola, S., Jacquemoud, S., & Gregoire, J. M. (2001). Detecting vegetation leaf water content using reflectance in the optical domain. *Remote Sensing of Environment*, *77*, 22–33.

Ceccato, P., Gobron, N., Flasse, S., Pinty, B., & Tarantola, S. (2002b). Designing a spectral index to estimate vegetation water content from remote sensing data: Part 1. Theoretical approach. *Remote Sensing of Environment*, *82*, 188–197.

Churkina, G., Tenhunen, J., Thornton, P., Falge, E., Elbers, J. A., Erhard, M., Grunwald, T., Kowalski, A., Rannik, U., & Sprinz, D. (2003). Analyzing the ecosystem carbon dynamics of four European coniferous forest using a biogeochemistry model. *Ecosystems*, *6*, 168–184.

Falge, E., Baldocchi, D., Olson, R., Anthoni, P., Aubinet, M., Bernhofer, C., Burba, G., Ceulemans, G., Clement, R., Dolman, H., Granier, A., Gross, P., Grunwald, T., Hollinger, D., Jensen, N. O., Katul, G., Keronen, P., Kowalski, A., Lai, C. T., Law, B. E., Meyers, T., Moncrieff, J., Moors, E., Munger, J. W., Pilegaard, K., Rannik, U., Rebmann, C., Suyker, A., Tenhunen, J., Tu, K., Verma, S., Vesala, T., Wilson, K., & Wofsy, S. (2001). Gap filling strategies for long term energy flux data sets. *Agricultural and Forest Meteorology*, *107*, 71–77.

Falge, E., Baldocchi, D., Tenhunen, J., Aubinet, M., Bakwin, P., Berbigier, P., Bernhofer, C., Burba, G., Clement, R., Davis, K. J., Elbers, J. A., Goldstein, A. H., Grelle, A., Granier, A., Guomundsson, J., Hollinger, D., Kowalski, A. S., Katul, G., Law, B. E., Malhi, Y., Meyers, T., Monson, R. K., Munger, J. W., Oechel, W., Paw, K. T., Pilegaard, K., Rannik, U., Rebmann, C., Suyker, A., Valentini, R., Wilson, K., & Wofsy, S. (2002a). Seasonality of ecosystem respiration and gross primary production as derived from FLUXNET measurements. *Agricultural and Forest Meteorology*, *113*, 53–74.

Falge, E., Tenhunen, J., Baldocchi, D., Aubinet, M., Bakwin, P., Berbigier, P., Bernhofer, C., Bonnefond, J. M., Burba, G., Clement, R., Davis, K. J., Elbers, J. A., Falk, M., Goldstein, A. H., Grelle, A., Granier, A., Grunwald, T., Gudmundsson, J., Hollinger, D., Janssens, I. A., Keronen, P., Kowalski, A. S., Katul, G., Law, B. E., Malhi, Y., Meyers, T., Monson, R. K., Moors, E., Munger, J. W., Oechel, W., Paw, U. K. T., Pilegaard, K., Rannik, U., Rebmann, C., Suyker, A., Thorgeirsson, H., Tirone, G., Turnipseed, A., Wilson, K., & Wofsy, S. (2002b). Phase and amplitude of ecosystem carbon release and uptake potentials as derived from FLUXNET measurements. *Agricultural and Forest Meteorology*, *113*, 75–95.

Field, C. B., Behrenfeld, M. J., Randerson, J. T., & Falkowski, P. (1998). Primary production of the biosphere: Integrating terrestrial and oceanic components. *Science*, *281*, 237–240.

Field, C. B., Randerson, J. T., & Malmstrom, C. M. (1995). Global net primary production—combining ecology and remote-sensing. *Remote Sensing of Environment*, *51*, 74–88.

Gao, B. C. (1996). NDWI—a normalized difference water index for remote sensing of vegetation liquid water from space. *Remote Sensing of Environment*, *58*, 257–266.

Gobron, N., Pinty, B., Verstraete, M., & Govaerts, Y. (1999). The MERIS Global Vegetation Index (MGVI): Description and preliminary application. *International Journal of Remote Sensing*, *20*, 1917–1927.

Gobron, N., Pinty, B., Verstraete, M. M., & Widlowski, J. L. (2000). Advanced vegetation indices optimized for up-coming sensors: Design, performance, and applications. *IEEE Transactions on Geoscience and Remote Sensing*, *38*, 2489–2505.

Goulden, M. L., Munger, J. W., Fan, S. M., Daube, B. C., & Wofsy, S. C. (1996). Exchange of carbon dioxide by a deciduous forest: Response to interannual climate variability. *Science*, *271*, 1576–1578.

Govaerts, Y. M., Verstraete, M. M., Pinty, B., & Gobron, N. (1999). Designing optimal spectral indices: A feasibility and proof of concept study. *International Journal of Remote Sensing*, *20*, 1853–1873.

Hanan, N., Kabat, P., Dolman, A. J., & Elbers, J. A. (1998). Photosynthesis and carbon balance of a Sahelian fallow savanna. *Global Change Biology*, *4*, 523–538.

Hanan, N. P., Burba, G., Verma, S., Berry, J. A., Suyker, A., & Walter-Shea, E. A. (2002). Inversion of net ecosystem CO_2 flux measurements for estimation of canopy PAR absorption. *Global Change Biology*, *8*, 563–574.

Huete, A., Didan, K., Miura, T., Rodriguez, E. P., Gao, X., & Ferreira, L. G. (2002). Overview of the radiometric and biophysical performance of the MODIS vegetation indices. *Remote Sensing of Environment*, *83*, 195–213.

Huete, A. R., Liu, H. Q., Batchily, K., & vanLeeuwen, W. (1997). A comparison of vegetation indices over a global set of TM images for EOS-MODIS. *Remote Sensing of Environment*, *59*, 440–451.

Hunt, E. R., & Rock, B. N. (1989). Detection of changes in leaf water-content using near-infrared and middle-infrared reflectances. *Remote Sensing of Environment*, *30*, 43–54.

Knyazikhin, Y., Martonchik, J. V., Myneni, R. B., Diner, D. J., & Running, S. W. (1998). Synergistic algorithm for estimating vegetation canopy leaf area index and fraction of absorbed photosynthetically active radiation from MODIS and MISR data. *Journal of Geophysical Research, [Atmospheres]*, *103*, 32257–32275.

Lambers, H., Chapin, F. S., & Pons, T. L. (1998). *Plant physiological ecology*. New York: Springer-Verlag.

Law, B. E., Waring, R. H., Anthoni, P. M., & Aber, J. D. (2000). Measure-

ments of gross and net ecosystem productivity and water vapour exchange of a *Pinus ponderosa* ecosystem, and an evaluation of two generalized models. *Global Change Biology*, *6*, 155–168.

Malmstrom, C. M., Thompson, M. V., Juday, G. P., Los, S. O., Randerson, J. T., & Field, C. B. (1997). Interannual variation in global-scale net primary production: Testing model estimates. *Global Biogeochemical Cycles*, *11*, 367–392.

Potter, C. S., Randerson, J. T., Field, C. B., Matson, P. A., Vitousek, P. M., Mooney, H. A., & Klooster, S. A. (1993). Terrestrial ecosystem production—a process model-based on global satellite and surface data. *Global Biogeochemical Cycles*, *7*, 811–841.

Prince, S. D., & Goward, S. N. (1995). Global primary production: A remote sensing approach. *Journal of Biogeography*, *22*, 815–835.

Raich, J. W., Rastetter, E. B., Melillo, J. M., Kicklighter, D. W., Steudler, P. A., Peterson, B. J., Grace, A. L., Moore, B., & Vorosmarty, C. J. (1991). Potential net primary productivity in South-America—application of a global-model. *Ecological Applications*, *1*, 399–429.

Ruimy, A., Dedieu, G., & Saugier, B. (1996). TURC: A diagnostic model of continental gross primary productivity and net primary productivity. *Global Biogeochemical Cycles*, *10*, 269–285.

Ruimy, A., Jarvis, P. G., Baldocchi, D. D., & Saugier, B. (1995). CO_2 fluxes over plant canopies and solar radiation: A review. *Advances in Ecological Research*, 1–68.

Ruimy, A., Kergoat, L., & Bondeau, A. (1999). Comparing global models of terrestrial net primary productivity (NPP): Analysis of differences in light absorption and light-use efficiency. *Global Change Biology*, *5*, 56–64.

Ruimy, A., Saugier, B., & Dedieu, G. (1994). Methodology for the estimation of terrestrial net primary production from remotely sensed data. *Journal of Geophysical Research, [Atmospheres]*, *99*, 5263–5283.

Running, S. W., Nemani, R., Glassy, J. M., & Thornton, P. (1999, April 29). MODIS daily photosynthesis (PSN) and annual net primary production (NPP) product (MOD17). *Algorithm theorectical basis document, version 3.0.* http://modis.gsfc.nasa.gov

Running, S. W., Thornton, P. E., Nemani, R., & Glassy, J. M. (2000). Global terrestrial gross and net primary productivity from the Earth Observing System. In O. E. Sala, R. B. Jackson, H. A. Mooney, & R. W. Howarth (Eds.), *Methods in ecosystem science* (pp. 44–57). New York: Springer.

Tucker, C. J. (1979). Red and photographic infrared linear combinations for monitoring vegetation. *Remote Sensing of Environment*, *8*, 127–150.

Turner, D. P., Ritts, W. D., Cohen, W. B., Gower, S. T., Zhao, M. S., Running, S. W., Wofsy, S. C., Urbanski, S., Dunn, A. L., & Munger, J. W. (2003a). Scaling gross primary production (GPP) over boreal and deciduous forest landscapes in support of MODIS GPP product validation. *Remote Sensing of Environment*, *88*, 256–270.

Turner, D. P., Urbanski, S., Bremer, D., Wofsy, S. C., Meyers, T., Gower, S. T., & Gregory, M. (2003b). A cross-biome comparison of daily light use efficiency for gross primary production. *Global Change Biology*, *9*, 383–395.

Waring, R. H., Landsberg, J. J., & Williams, M. (1998). Net primary production of forests: A constant fraction of gross primary production? *Tree Physiology*, *18*, 129–134.

Waring, R. H., Law, B. E., Goulden, M. L., Bassow, S. L., Mccreight, R. W., Wofsy, S. C., & Bazzaz, F. A. (1995). Scaling gross ecosystem production at Harvard Forest with remote-sensing—a comparison of estimates from a constrained quantum-use efficiency model and Eddy-correlation. *Plant, Cell & Environment*, *18*, 1201–1213.

Williams, M., Rastetter, E. B., Fernandes, D. N., Goulden, M. L., Shaver, G. R., & Johnson, L. C. (1997). Predicting gross primary productivity in terrestrial ecosystems. *Ecological Applications*, *7*, 882–894.

Wilson, K. B., Baldocchi, D. D., & Hanson, P. J. (2001). Leaf age affects the seasonal patterns of photosynthetic capacity and net ecosystem exchange of carbon in a deciduous forest. *Plant, Cell & Environment*, *24*, 571–583.

Wofsy, S. C., Goulden, M. L., Munger, J. W., Fan, S. M., Bakwin, P. S., Daube, B. C., Bassow, S. L., & Bazzaz, F. A. (1993). Net exchange of CO_2 in a midlatitude forest. *Science*, *260*, 1314–1317.

Xiao, X., Boles, S., Liu, J. Y., Zhuang, D. F., & Liu, M. L. (2002). Characterization of forest types in Northeastern China, using multi-temporal SPOT-4 VEGETATION sensor data. *Remote Sensing of Environment*, *82*, 335–348.

Xiao, X., Braswell, B., Zhang, Q., Boles, S., Frolking, S., & Moore, B. (2003). Sensitivity of vegetation indices to atmospheric aerosols: Continental-scale observations in northern Asia. *Remote Sensing of Environment*, *84*, 385–392.

Xiao, X., Hollinger, D., Aber, J. D., Goltz, M., Davidson, E. A., & Zhang, Q. Y. (2004). Satellite-based modeling of gross primary production in an evergreen needleleaf forest. *Remote Sensing of Environment*, *89*, 519–534.

Zarco-Tejada, P. J., Rueda, C. A., & Ustin, S. L. (2003). Water content estimation in vegetation with MODIS reflectance data and model inversion methods. *Remote Sensing of Environment*, *85*, 109–124.